ADVANCED HEALTHCARE MATERIALS
www.advhealthmat.de

Highly Resilient Noncovalently Associated Hydrogel Adhesives for Wound Sealing Patch

*Gi-Yeon Han, Ji-Yong Park, Jong-Ho Back, Mo-Beom Yi, and Hyun-Joong Kim**

The development of hydrogel adhesives with high mechanical resilience and toughness remains a challenging task. Hydrogels must exhibit high mechanical resilience to withstand the inevitable movement of the human body while simultaneously demonstrating strong wet tissue adhesion and appropriate toughness to hold and seal damaged tissues; However, tissue adhesion, toughness, and mechanical resilience are typically negatively correlated. Therefore, this paper proposes a highly resilient double-network (DN) hydrogel wound-sealing patch that exhibits a well-balanced combination of tissue adhesion, toughness, and mechanical resilience. The DN structure is formed by introducing covalently and non-covalently crosslinkable dopamine-modified crosslinkers and physically interactable linear poly(vinyl imidazole) (PVI). The resulting hydrogel adhesive exhibits high toughness and mechanical resilience due to the presence of a DN involving reversible physical intermolecular interactions such as hydrogen bonds, hydrophobic associations, cation–π interactions, π–π interactions, and chain entanglements. Moreover, the hydrogel adhesive achieves strong wet tissue adhesion through the polar hydroxyl groups of dopamine and the amine group of PVI. These mechanical attributes allow the proposed adhesive to effectively seal damaged tissues and promote wound healing by maintaining a moist environment.

1. Introduction

Hydrogel adhesives are widely used as wound closure patches due to their high similarity to living tissues.[1] In comparison with surgical stitching, the use of hydrogel adhesives can prevent secondary tissue damage and reduce time consumption[2,3]; However, hydrogel adhesives typically lack the adhesiveness and toughness required for securely holding and sealing wounds.[4]

In recent years, hydrogel adhesives with diverse functionalities, such as high toughness,[5,6] stretchability,[7,8] and self-healability[9,10] have been reported. However, most existing studies focus on only one specific property. Notably, to ensure the practical use of hydrogel adhesives as wound-sealing patches, a well-balanced combination of tissue adhesion, toughness, and mechanical resilience is required, posing a challenge due to the negative correlation among these characteristics.[11]

The primary challenge in the development of hydrogel adhesives is the simultaneous realization of strong wet tissue adhesion and high mechanical resilience. Wounded tissues produce large amounts of exudate, and joint areas and organs are frequently subjected to a wide range of motions.[12–14] For hydrogel adhesives to be used as wound-sealing patches, they must strongly adhere to wet tissues and adapt to dynamic movements without deformation.[15,16] Insufficient adhesion and mechanical resilience of hydrogel adhesives can lead to poor contact with dynamic wound sites, which increases the risk of secondary infection[14] and limits their long-term use.[17]

Double-network (DN) hydrogels can simultaneously achieve high toughness and mechanical resilience through their heterogeneous network structures.[18] Specifically, DN hydrogels consist of a highly crosslinked first network that maintains their shape and a slightly crosslinked/entangled second network that dissipates energy. When mechanical stress is applied, the second network redistributes energy, while the first network maintains its elasticity.[19,20] Furthermore, if the applied stress exceeds the capacity of the first network, the fragments of the disrupted first network can act as crosslinkers for the second network.[21]

As a result, DN hydrogels exhibit significantly increased toughness compared to single-network hydrogels. In recent years, the introduction of reversible bonds such as host–guest interactions,[22] hydrophobic associations,[23] Schiff-base reactions,[24] interpenetrating structures,[25] and crystalline structures,[26] has enabled DN hydrogels to achieve high toughness with excellent elasticity.

Notably, toughness and adhesiveness are typically negatively correlated. As the toughness of an adhesive increases, its ability to wet the interface between substrates and adhesives decreases.[27] To address this trade-off relationship,[28,29]

G.-Y. Han, J.-H. Back, M.-B. Yi, H.-J. Kim
Program in Environmental Materials Science
Department of Agriculture, Forestry and Bioresources
Seoul National University
Seoul 08826, Republic of Korea
E-mail: hjokim@snu.ac.kr
J.-Y. Park
Department of Veterinary Physiology
College of Veterinary Medicine
Seoul National University
Seoul 08826, Republic of Korea

The ORCID identification number(s) for the author(s) of this article can be found under https://doi.org/10.1002/adhm.202303342

DOI: 10.1002/adhm.202303342

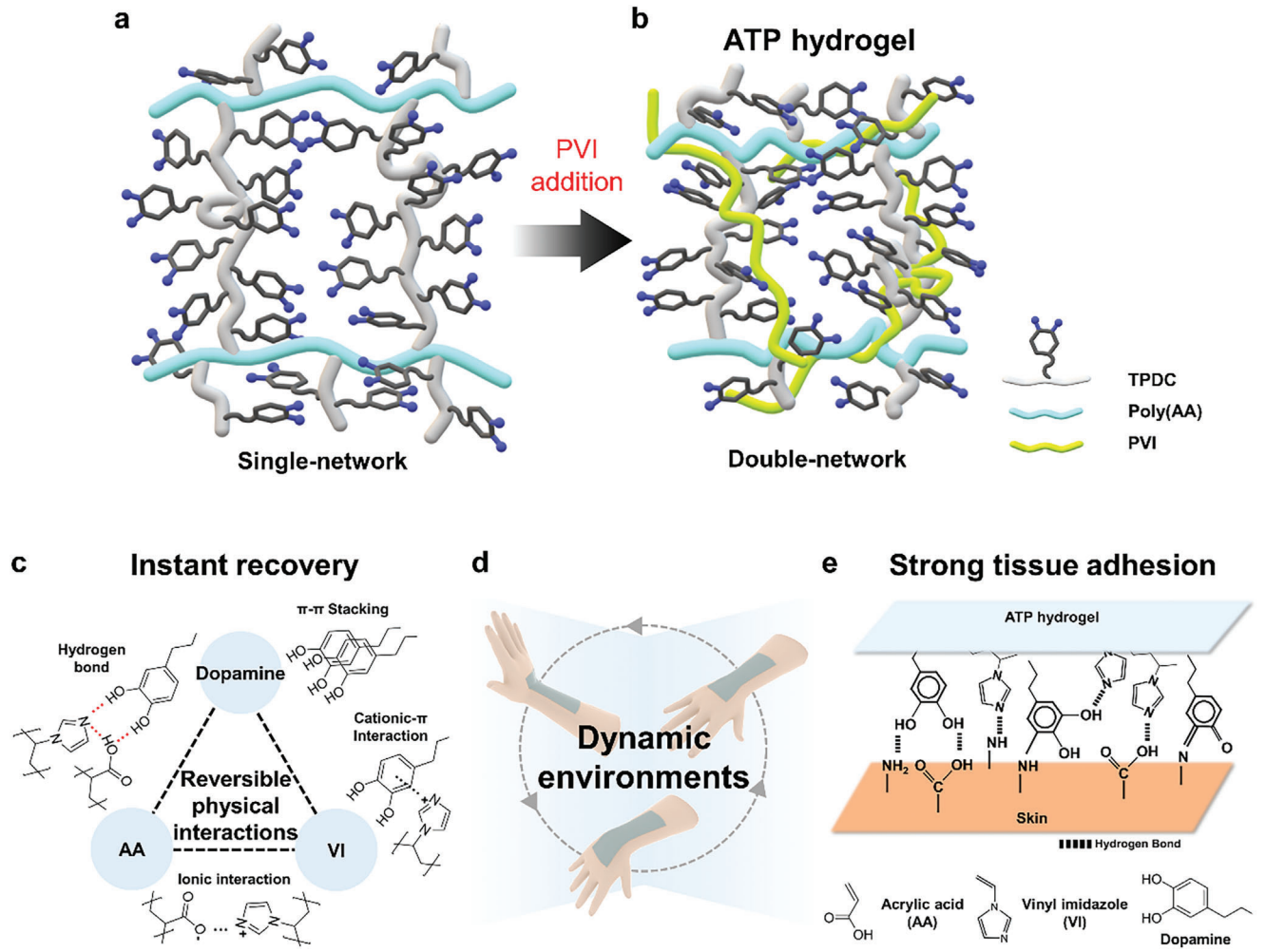

Figure 1. Schematic of the ATP hydrogel network structure a) without PVI and b) with PVI. c) Reversible physical interactions between dopamine, poly(AA), and PVI. d) Schematic of hydrogel adhesives applied to dynamic body parts. e) Adhesion mechanism between tissues and ATP hydrogel.

dopamine-modified crosslinkers were introduced in our previous study.[30] In this framework, acrylate-terminated and dopamine-modified crosslinkers underwent covalent crosslinking with acrylate, and the dopamine molecules in the crosslinkers generated reversible physical crosslinking and hydrogen bonding with tissues. Although the hydrogel adhesives prepared using dopamine-modified crosslinkers achieved high mechanical resilience and strong tissue adhesion, their elongation was limited due to the hydrogel network being formed only by covalent bonds.

This study was aimed to develop highly resilient DN hydrogel adhesives characterized by high wet tissue adhesion and toughness, enabling their application in dynamic environments. The DN structure was formed using a dopamine-modified crosslinker, specifically the tri(propylene glycol) diacrylate-dopamine crosslinker (TPDC), and linear poly(vinyl imidazole) (PVI). The first network was formed through the multiple crosslinking of TPDC, involving covalent bonds, hydrophobic associations, π–π stacking, and hydrogen bonds (**Figure 1a**). The second network was established through additional intermolecular interactions induced by PVI addition, such as chain entanglement, cation–π interactions, and hydrogen bonds (Figure 1b). The network structures were noncovalently associated by reversible physical interactions between poly(acrylic acid) (AA), TPDC, and PVI (Figure 1c). The resulting hydrogel, named acrylic acid-TPDC-PVI (ATP) hydrogel, exhibited excellent stretchability and instant recovery properties through the noncovalently associated network structure. The hydroxyl group of dopamine and the amine group of PVI, exposed on the hydrogel surface, formed hydrogen bonds and participated in Schiff-base reactions with the wet tissue surface, ensuring the strong wet tissue adhesion of the ATP hydrogel (Figure 1e). Moreover, the pH-sensitive AA allowed the hydrogel to maintain a moist environment by absorbing excess exudates produced from the wound site, promoting wound healing. Through these well-balanced mechanical characteristics, the ATP hydrogel can withstand successive cyclic loading and effectively seal damaged tissues. Consequently, ATP hydrogel has the potential to be utilized as a wound-sealing patch in dynamic tissues of the human body (Figure 1d).

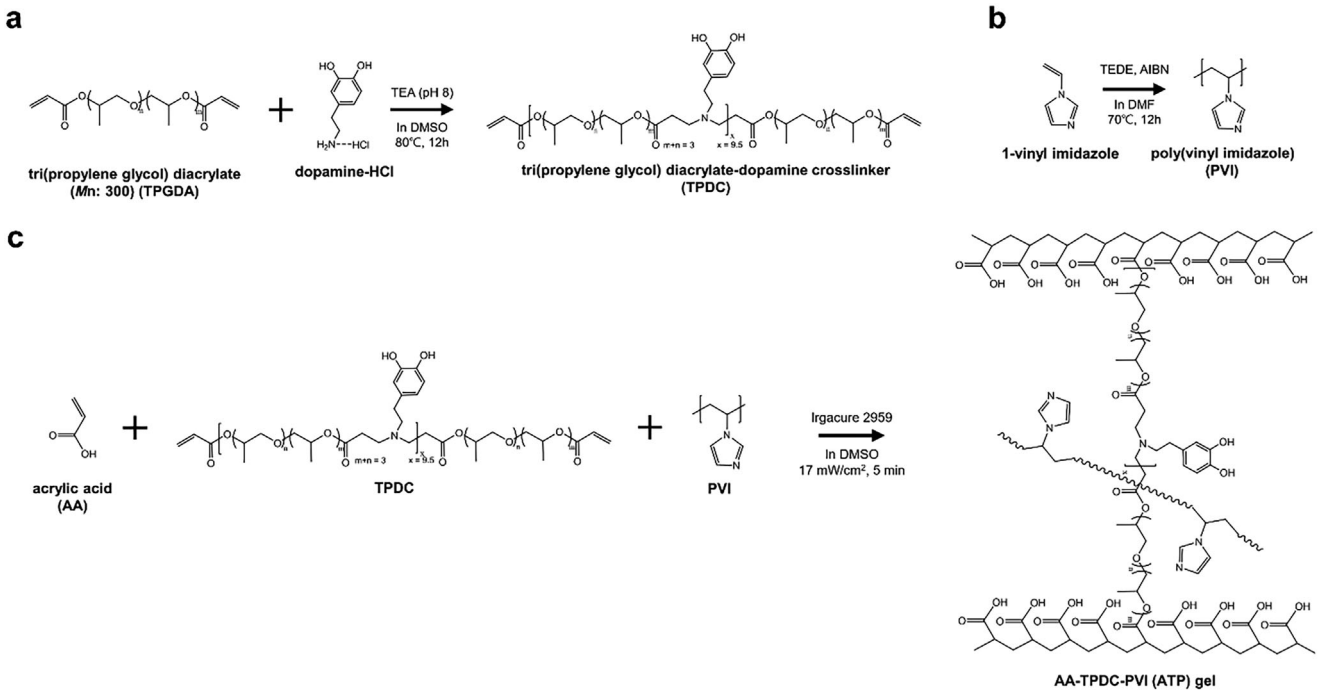

Figure 2. Chemical synthesis process of a) TPDC, b) PVI, and c) ATP gel.

2. Results and Discussion

2.1. Preparation of Crosslinker and Hydrogel

TPDC was synthesized via the aza-Michael reaction, with the molar ratio of tri (propylene glycol) diacrylate and dopamine hydrochloride was set as 1.1: 0.5 (**Figure** 2a). This reaction was completed in 9 h, as indicated by the reduction in the acrylate C═C bond band (810 cm^{-1}) of in the Fourier transform-infrared (FT-IR) spectrum (Figure S1, Supporting Information). The end-group fidelity of the product was confirmed by the acrylate C═C bond proton peaks (5.9–6.4 ppm) in the proton nuclear magnetic resonance (^{1}H NMR) spectrum (Figure S2, Supporting Information). The molecular weight of TPDC was calculated using the proton peak integral values between 5.9–6.0 ppm (acrylate C═C) and 6.55–6.75 ppm (benzene CH, adjacent to OH). The peak integral ratio of the 5.9–6.0 ppm peaks to 6.55–6.75 ppm peaks is 1: 9.5, indicating the incorporation of ≈9.5 dopamine molecules in each TPDC. Thus, the average molecular weight of TPDC was estimated to be 4 600. PVI was synthesized through reversible addition−fragmentation chain-transfer polymerization (Figure 2b). Reaction was confirmed by the disappearance of vinyl C═C bond proton peaks (4.8–5.6 ppm) of ^{1}H NMR spectroscopy (Figure S3, Supporting Information). The DN hydrogel is prepared following two steps: 1) radical polymerization of acrylate, and 2) solvent exchange. First, the synthesized TPDC was copolymerized with AA using dimethyl sulfoxide (DMSO) as a solvent. In this step, PVI was employed to form the second network with physical crosslinking (Figure 2c). Next, the prepared gel was immersed in cold deionized water (DIW) for 24 h to remove any unreacted monomers and DMSO. The unreacted monomers and DMSO were fully extracted after 7 h (Figure S4, Supporting Information), and the ATP hydrogel was obtained. The hydrogel with x wt.% of PVI was denoted as the ATPx hydrogel.

2.2. Characterization of DN Hydrogels

The prepared ATP hydrogel comprises two networks. The first network involves the covalently crosslinked TPDC (Figure 1a), along with noncovalent bonds, such as hydrophobic associations (propylene glycol and dopamine) and hydrogen bonds (poly(AA) and dopamine) (Figure 1c). The second network consists of physically crosslinked PVI (Figure 1b). Linear PVI induces physical crosslinking through chain entanglement and intermolecular interactions such as hydrogen bonding, hydrophobic interactions, π–π stacking, and cation–π interactions (Figure 1c). The effect of PVI on the formation of the second network was confirmed by variations in the swelling ratio and surface atomic ratio of the ATP hydrogel with changes in the PVI content. The ATP0 hydrogel (without PVI) swelled by ≈30%, whereas the other hydrogels (with various PVI contents) contracted. As the PVI content increased, the hydrogel contraction ratio gradually increased from ≈20% (ATP1 hydrogel) to 50% (ATP4 hydrogel) (**Figure** 3a), and the water content correspondingly decreased from ≈76% (ATP0 hydrogel) to 38% (ATP4 hydrogel) (Figure 3b). The surface atomic ratios of the ATP hydrogels were determined through X-ray photoelectron spectroscopy (XPS) (Figure S5, Supporting Information). As the PVI content increased, the proportion of C—O bonds increased from 17.0% (ATP0 hydrogel) to 26.2% (ATP4 hydrogel) (Figure 3c–e). Specifically, as intermolecular interactions such as hydrogen bonds, hydrophobic associations, cation–π interactions, and chain entanglements increased, the hydrophilic moieties (hydroxyl group of dopamine and amine

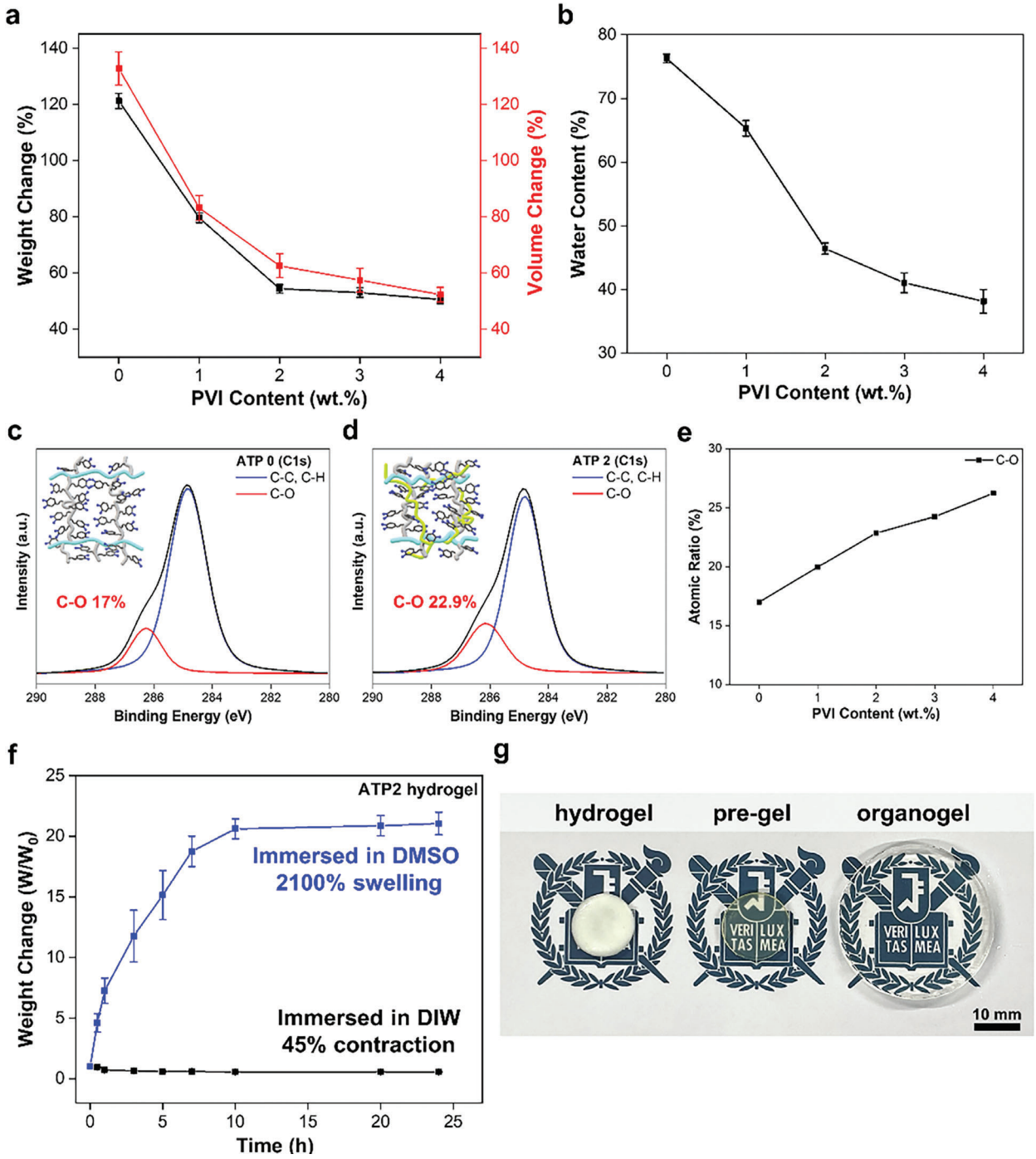

Figure 3. a) Change in the weight and volume of the ATP pre-gel when immersed in DIW for 24 h. b) Water content of the ATP hydrogels with different PVI contents. Peak-fitting XPS spectra of c) ATP0 hydrogel and d) ATP2 hydrogel. e) Atomic ratios of ATP hydrogel calculated using the corresponding XPS spectra. f) Change in the weight of the ATP2 pre-gel when immersed in DMSO and DIW. g) Photographs of the ATP2 pre-gel, hydrogel (immersed in DIW) and organogel (immersed in DMSO).

group of imidazole) became more exposed to the hydrogel surface as the hydrophobic moieties (propylene glycol and benzene ring of dopamine) became more associated within the hydrogel network. In other words, the addition of PVI enhanced the intermolecular interactions in the bulk layer, resulting in a denser network structure of the ATP hydrogel.

The ATP hydrogel network consisted of two main types of bonds: covalent bonds formed by the acrylate, and noncovalent bonds formed between poly(AA), TPDC, and PVI. To evaluate the effect of these noncovalent intermolecular interactions such as hydrogen bonds, hydrophobic associations, cation–π interactions, π–π interactions, and chain entanglements on the

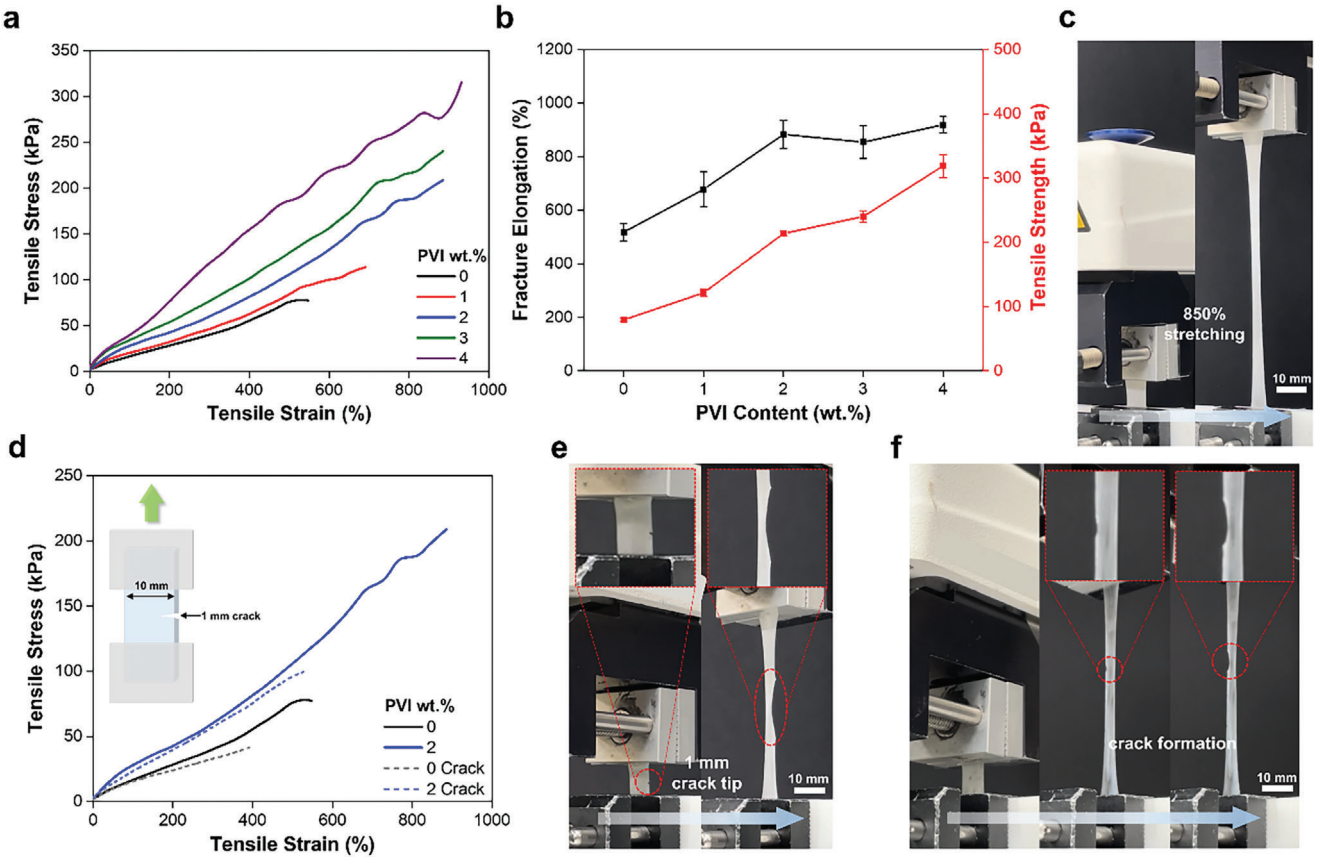

Figure 4. a) Strain–stress curves of the ATP hydrogels with different PVI contents. b) Fracture elongation and tensile strength of the ATP hydrogels with different PVI contents. c) Photographs of the stretched ATP2 hydrogel. d) Stress–strain curve of notched ATP0 and ATP2 hydrogels and e) photographs of notched ATP2 hydrogel. f) Photographs of stretched ATP4 hydrogel.

formation of the hydrogel network, ATP2 pre-gel was immersed in DMSO and DIW for 24 h, and the weight change of the pre-gel was observed. DMSO, which is amphiphilic owing to the presence of a polar sulfoxide group and nonpolar methyl group, weakens the hydrogen bonds, hydrophobic associations, cation–π interactions, and π–π interactions of the ATP hydrogel.[31] The weight of the ATP2 pre-gel increased and decreased by ≈2100% and 55% with respect to its original weight when immersed in DMSO and DIW, respectively (Figure 3f). Moreover, comparing the gels immersed in each solvent, ATP hydrogel is opaque and ATP organogel is transparent (Figure 3g). This difference in light transmittance is caused by the association of polymer network structure forming light scattering centers. These results demonstrate that noncovalent intermolecular interactions between poly(AA), TPDC, and PVI influence the formation of the hydrogel network, making it denser.[32,33]

2.3. Mechanical Performances

Because the mechanical properties of hydrogels are affected by the corresponding hydrogel network structure, tensile tests were conducted to examine the change in the mechanical properties with varying PVI contents (0 wt.% to 5 wt.%) (Movie S1, Supporting Information). The addition of PVI, which formed the second network through physical crosslinking, increased the fracture elongation and tensile strength of the ATP hydrogels. The fracture elongation and tensile strength of the ATP0 hydrogel were 510% and 80 kPa, respectively, whereas the corresponding value for the ATP4 was dramatically increased to 910% and 310 kPa (**Figure** 4a–c). The physically crosslinked networks of the hydrogel dissociated under mechanical stress, resulting in energy dissipation and redistribution energy, thereby the fracture elongation and tensile strength were increased with the increase in PVI content. The effect of the DN structure on the mechanical properties of the ATP hydrogels was evaluated through crack tip tests. The PVI-containing DN hydrogel (ATP2 hydrogel) was ≈150% more elongated than the single-network hydrogel (ATP0 hydrogel). The higher crack propagation resistance of the ATP2 hydrogel was attributable to the effective redistribution of stress around the crack tip by the DN network (Figure 4d,e).[20] The fracture elongation limit of the PVI-containing hydrogels (ATP2–4 hydrogels) was observed to be 900%, beyond which, the network structure could no longer withstand mechanical loading. At elongations exceeding 600%, fluctuations in the strain–stress curve were observed in the PVI-containing ATP hydrogels (ATP1–4 hydrogels). These fluctuations were attributable to the occurrence of necking and crack generation in the hydrogel as the first network was destroyed, which intensified with further stretching of the hydrogel (Figure 4f).[21]

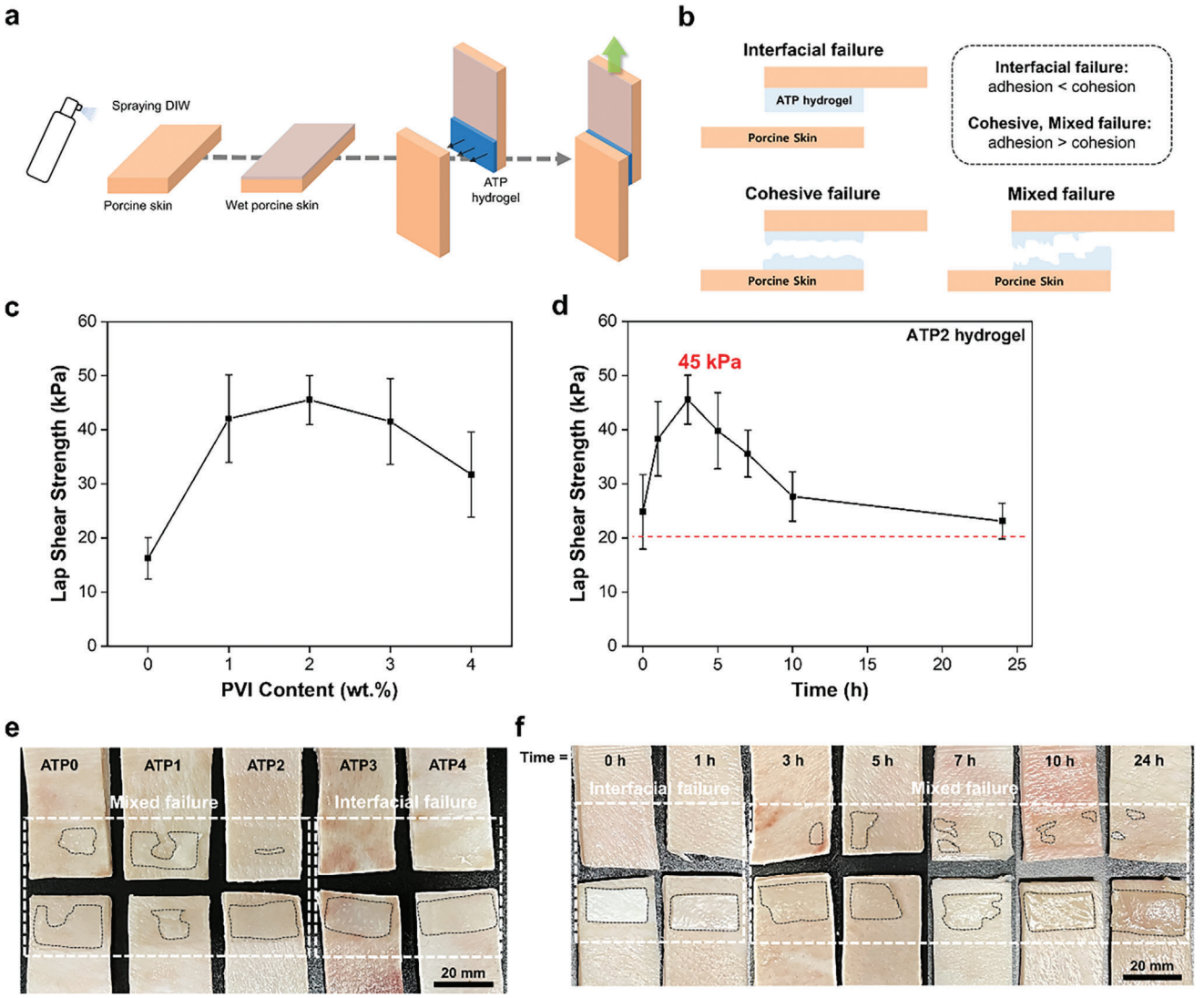

Figure 5. a) Schematic of the lap shear test process and b) failure modes of adhesive after adhesion test. c) Tissue adhesion strength of ATP hydrogels with different PVI contents and d) change in the tissue adhesion strength of the ATP2 hydrogel over time. e) Failure mode of the ATP hydrogels after lap shear tests with different PVI contents. f) Failure mode of the ATP2 hydrogel at different time points after adhesion. Grey dashed lines represent the residual ATP hydrogels on the porcine skin after lap shear test.

2.4. Adhesion Performances

The adhesion strength of the ATP hydrogels was evaluated by conducting lap shear test (**Figure 5**a; Movie S2, Supporting Information) and observing the failure mode of the ATP hydrogels. The failure mode of an adhesive is determined by the balance between its adhesion and cohesion forces. Analyzing the adhesion strength and failure modes reveals the mechanical performance of the adhesive (Figure 5b). Porcine skin was selected as the model tissue owing to its similarity to human skin.[34] To simulate a wet physiological environment, the ATP hydrogels were attached to fully wetted porcine skin and stored in wet conditions. The addition of PVI significantly increased the adhesion strength from 16.2 kPa (ATP0 hydrogel) to 42.1 kPa (ATP1 hydrogel) with a linear progression to 45.5 kPa (ATP2 hydrogel) up to an added content of 2 wt.% (Figure 5c). Specifically, the addition of PVI increased the amount of amine group of imidazole and promoted the exposure of the hydroxyl group of dopamine to the hydrogel surface (Figure 3e). Therefore, the adhesion strength was expected to increase with the PVI content. However, when the PVI addition content exceeded 3 wt.%, the adhesion strength decreased to 31.7 kPa (ATP4 hydrogel). This phenomenon occurred because the hydrogen bonds, hydrophobic associations, cation–π interactions, and chain entanglements were intensified by the addition of PVI, which increased the modulus of the hydrogel. The elevated modulus led to reduced wettability, resulting in the decreased adhesion strength of the hydrogel.[29] The increase in modulus was confirmed by the strain–stress curve of the ATP hydrogels (Figure 4a) and the failure modes. As the PVI content increased, their failure modes changed from a mixed failure mode (ATP0–2 hydrogels) to interfacial failure (ATP3 and ATP4 hydrogels) (Figure 5e). These results demonstrate that ATP hydrogels

robustly adhere to biological tissues and adhesion strength varies with PVI contents as the modulus of the hydrogel changes.

2.5. Change in Adhesion Strength over Time

When a hydrogel is implanted in the human body, it is exposed to wet conditions induced by the exudate produced by damaged skin and sweat from everyday activities. Therefore, hydrogel adhesives must maintain adhesion in wet environments to ensure their durability. To evaluate the adhesion maintenance of the ATP hydrogel, the change in the tissue adhesion over time (0, 1, 3, 6, 10, and 24 h) under wet conditions was observed using the ATP2 hydrogel, which exhibited the highest adhesion strength among the prepared hydrogels. The initial adhesion strength was 24.8 kPa, which gradually increased to the peak value of 45.5 kPa 3 h after adhesion (Figure 5d). The exposed hydroxyl group of dopamine and amine group of PVI formed hydrogen bonds with the functional groups present in the skin, such as the amine, carboxylic acid, and hydroxyl groups. Therefore, the ATP hydrogel exhibited high tissue adhesion in the initial stages. Over time, oxidation and Schiff-base reactions of dopamine occurred, resulting in the formation of strong bonds between the skin and increased adhesion strength.[35] Within 1 h post-adhesion, insufficient interactions occurred between the ATP hydrogel and skin, leading to interfacial failure of the hydrogel. (Figure 5f). However, as the interactions between the ATP hydrogel and skin intensified up to 3 h after adhesion, the failure mode of the ATP hydrogel transitioned to a mixed failure mode. As the attachment duration exceeded 3 h, the adhesion strength decreased (e.g., 27.6 kPa after 10 h). Nevertheless, the ATP hydrogel exhibited adhesion strengths of over 20 kPa even after 24 h of adhesion. The decrease in adhesion strength is attributable to the decrease in cohesion of the ATP hydrogel owing to water absorption and hydrogel degradation. As the adhesion time increases, additional interactions between the ATP hydrogel and substrate are formed, but these interactions also weaken the existing interactions within ATP hydrogel network.[36] Therefore, the dissociation of the network structure occurred as adhesion duration increased, resulting in the cohesion of the ATP hydrogel, which is the strength itself, decreasing. Since the adhesion strength is determined by a combination of cohesive and adhesive forces, a decrease in cohesion results in a decrease in adhesion strength.[37] This phenomenon (dissociation of the ATP hydrogel network structure) can be indirectly observed by the change in transparency of the ATP hydrogel according to adhesion time. The ATP hydrogel changes from opaque to transparent due to the disappearance of the light scattering center caused by the dissociation of the ATP hydrogel network structure (Figure 5f).

2.6. Recovery Performance

The human body contains numerous mobile components: Joints such as the knee, wrist, and ankle exhibit a wide range of motion; and organs such as the lungs, heart, and tendons repeatedly contract and relax. Hence, hydrogels must exhibit high mechanical resilience to withstand dynamic mechanical loadings.[38,39] To evaluate the recovery property of the ATP2 hydrogel in dynamic environments, a cyclic tensile test was conducted without rest. The residual strain and resilience were calculated using the initial loading–unloading curves at different strain rates (**Figure 6**a). The ATP2 hydrogel exhibited a low residual strain (≈35%) and high mechanical resilience (≈63%) at strain rates of 200% and 400% (Figure 6b,c). At strain rates exceeding 600%, i.e., 700%, the mechanical resilience decreased to 53%, and the residual strain increased to 85% (Figure 6d,e). The recovery performance of the ATP hydrogel was attributable to the associated TPDC and entangled PVI: The associated TPDC can reversibly reassociate when mechanical stress is removed, and entangled PVI can enhance the elasticity of the hydrogel.[40] Owing to its noncovalently associated DN structure, the ATP hydrogel demonstrated excellent recovery properties even without external stimuli. Notably, at strain rates exceeding 600%, the resilience significantly decreased, and the residual strain increased owing to the irreversible destruction of the covalently crosslinked network structure (Figure 6f); However, even after the destruction of the first network (covalent crosslinking), its fragments functioned as crosslinkers of the second network,[21] and hydrogen bonds, hydrophobic associations, cation–π interactions, and chain entanglements induced by PVI contributed to the elasticity of the ATP hydrogel to a certain extent. Therefore, the ATP hydrogel exhibited excellent recovery properties even at high strain rates. Finally, successive cycle tensile test was conducted to demonstrate the applicability of the ATP hydrogel at joint areas. The strain rate was set at 100%, considering the maximum strain rates of human motions,[38,41] and the test was conducted for 200-cycles. The ATP2 hydrogel could withstand 200-cycles at strain rate of 100% (Figure 6g) and exhibited high mechanical resilience even after 200-cycles (Figure 6f). These results demonstrate the stability of the ATP2 hydrogel in dynamic environments.

2.7. Burst Pressure and Potential Applications

The burst pressure test is an effective method for evaluating the robustness of hydrogel adhesives against dynamic pressure and their adhesiveness at wound sites (**Figure 7**a).[42] As the PVI content increased, the burst pressure of the ATP hydrogel increased from 114 mmHg (ATP0 hydrogel) to 236 mmHg (ATP4 hydrogel) (Figure 7b). Higher PVI content increases the toughness of the ATP hydrogel, leading to enhanced burst pressure strength. The burst pressure of the ATP hydrogel was higher than that of commercial sealing adhesives (under 50 mmHg).[4,13] Considering normal human arterial blood pressure (typically 120 mmHg), PVI-containing ATP hydrogels (ATP1–4 hydrogels) exhibited excellent pressure resistance, exceeding 160 mmHg.

A water/air sealing test using an ex vivo porcine model was conducted to evaluate the potential applications of the hydrogel. Perforations were created in the porcine small intestine and lung, and water and air flow were introduced, respectively. The damaged areas were then sealed using the ATP2 hydrogel. The ATP2 hydrogel effectively sealed the damaged spots even when water and air were still flowing, owing to its strong tissue adhesion and high toughness. (Figure 7c,d; Movies S3 and S4, Supporting Information). Furthermore, the sealing performance of the ATP2 hydrogel in physiological conditions was evaluated using a porcine small intestine. The perforated porcine small

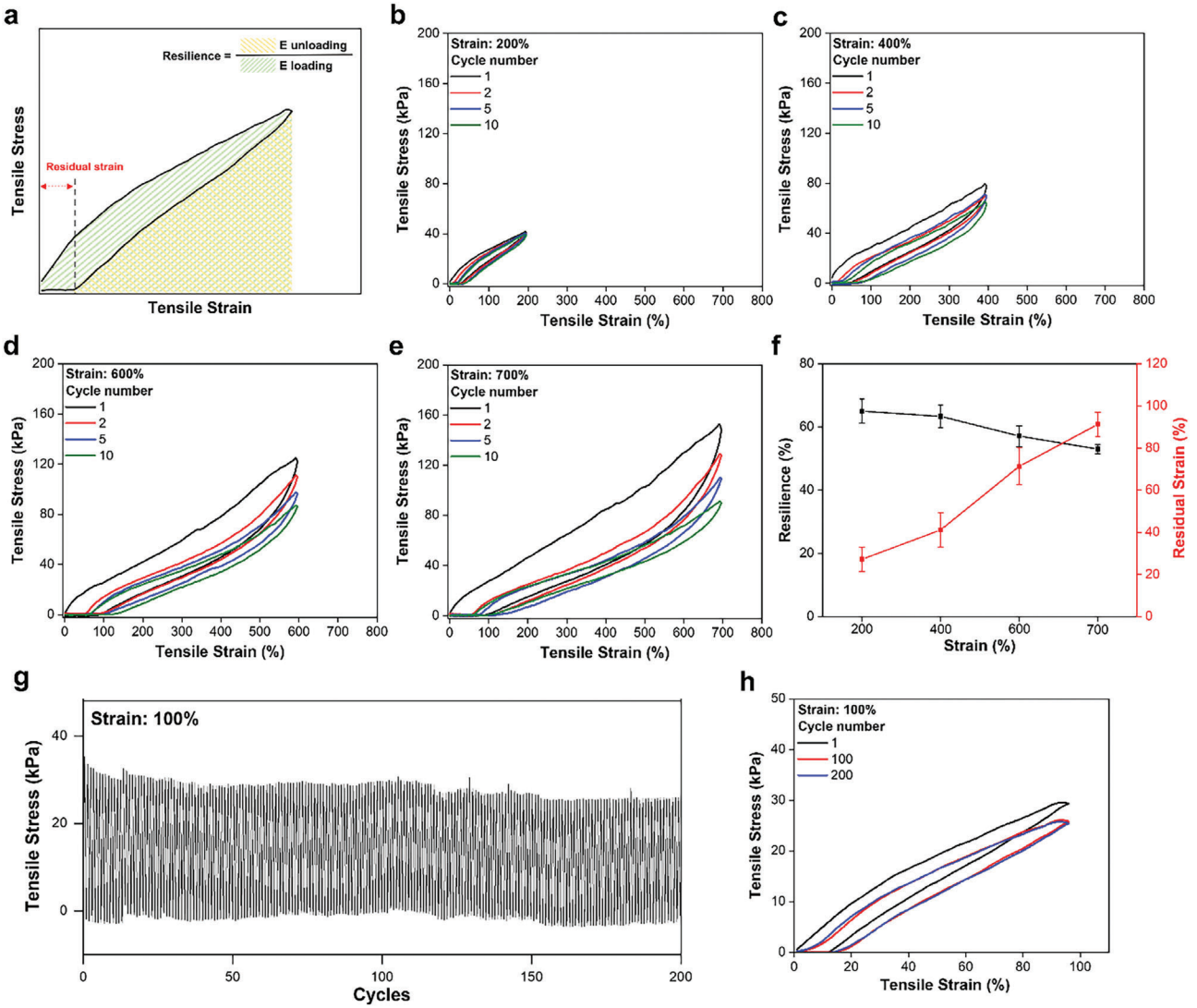

Figure 6. a) Schematic of tensile hysteresis curve. Stress–strain curves of the cyclic tensile tests of the ATP2 hydrogel at strain rates of b) 200%, c) 400%, d) 600%, and e) 700%; and f) resilience and residual strain at different strain rates. g) The successive cycle tensile test of ATP2 hydrogel at strain rate 100% and h) stress–strain curves of its 1st, 100th, and 200th cycle.

intestine sealed with the ATP2 hydrogel was immersed in Phosphate Buffered Saline (PBS) solution (pH 7.4) for 48 h. The inside of the small intestine was filled with red PBS solution stained with Direct Red 80 dye for visual effect. The high wet tissue adhesion of the ATP hydrogel sealed the perforation effectively in a moist environment. Over time, due to the pH-sensitive AA and the hydrolysable ester bond in TPDC, the ATP2 hydrogel swells and degrades. However, no liquid leakage was observed over 36 h due to the ATP2 hydrogel forming robust adhesion at the interface of the hydrogel and biological tissues (Figure 7e). These results demonstrate the sealing performance and stability in a physiological environment of the ATP2 hydrogel.

Compared to existing hydrogel adhesives, the proposed ATP2 hydrogel adhesive demonstrated enhanced and well-balanced mechanical properties. Specifically, ATP2 hydrogel adhesives demonstrate robust wet tissue adhesion (45.5 kPa) and high tensile strength (213.8 kPa), along with significant fracture elongation (883.5%) (Figure S6, Supporting Information). These well-balanced mechanical properties enabled the ATP2 hydrogel to achieve a higher burst pressure (174.7 kPa) compared to commercially available fibrin, polyethylene glycol, and cyanoacrylate glues.[4,24,43,44] To assess the biocompatibility and wound healing capabilities, both in vitro and in vivo tests were conducted using the ATP2 hydrogel, which exhibited optimal mechanical performance.

2.8. Biocompatibility

The biocompatibility of the ATP hydrogel was confirmed through in vitro biodegradation and cell tests. Biodegradability was assessed by immersing the ATP hydrogel in a PBS solution at 36 °C. ATP2 hydrogel exhibit 49% degradation after 36 h and completely degrading after 72 h (**Figure 8a**) due to the hydrolysable ester

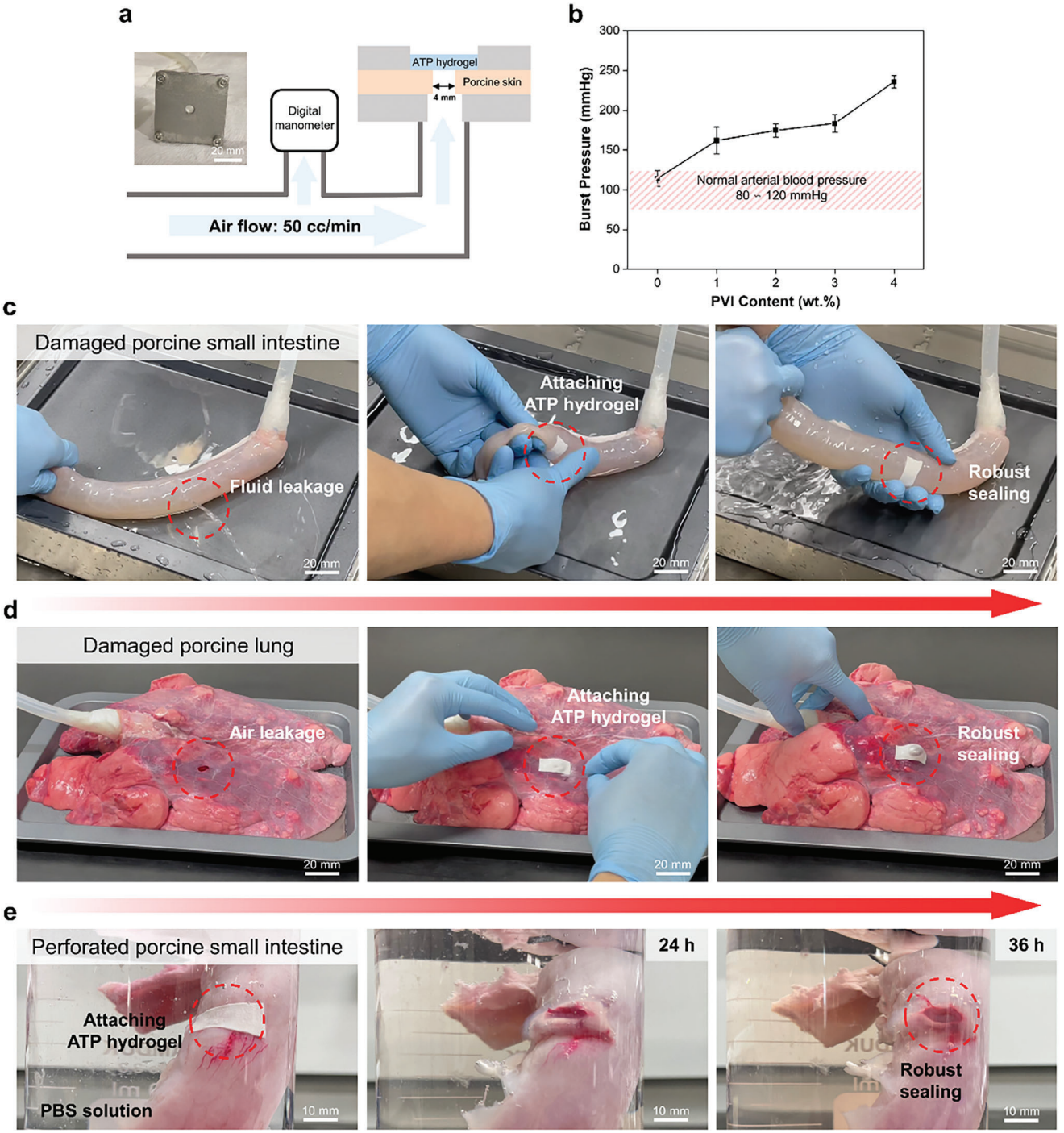

Figure 7. a) Schematic of the burst pressure test process. b) Burst pressures of the ATP hydrogels with different PVI contents. Photographs of c) fluid leakage sealing and d) air leakage sealing tests using the ATP2 hydrogel. e) Photographs of sealing performance tests of the ATP2 hydrogel.

bond in the TPDC (Figure 8b). To assess potential toxicity of the ATP hydrogel, the impact of its degradation products on STO cells over time (Figure 8c). In comparison to the control group, the hydrogel-treated group exhibited no significant difference in cell viability (Figure 8d) and cytotoxicity (Figure 8e). In summary, the ATP hydrogel degrades under physiological conditions, and its degradation products do not pose harm to the cells.

2.9. Wound Healing Performance

The wound healing performance of the ATP hydrogel was assessed using a rat wound model, monitoring changes in wound size over time (0, 4, 8, and 11 d post-implantation). Subsequently, histological analyses (immunohistochemistry (IHC), hematoxylin-eosin (H&E), and Masson's trichrome staining)

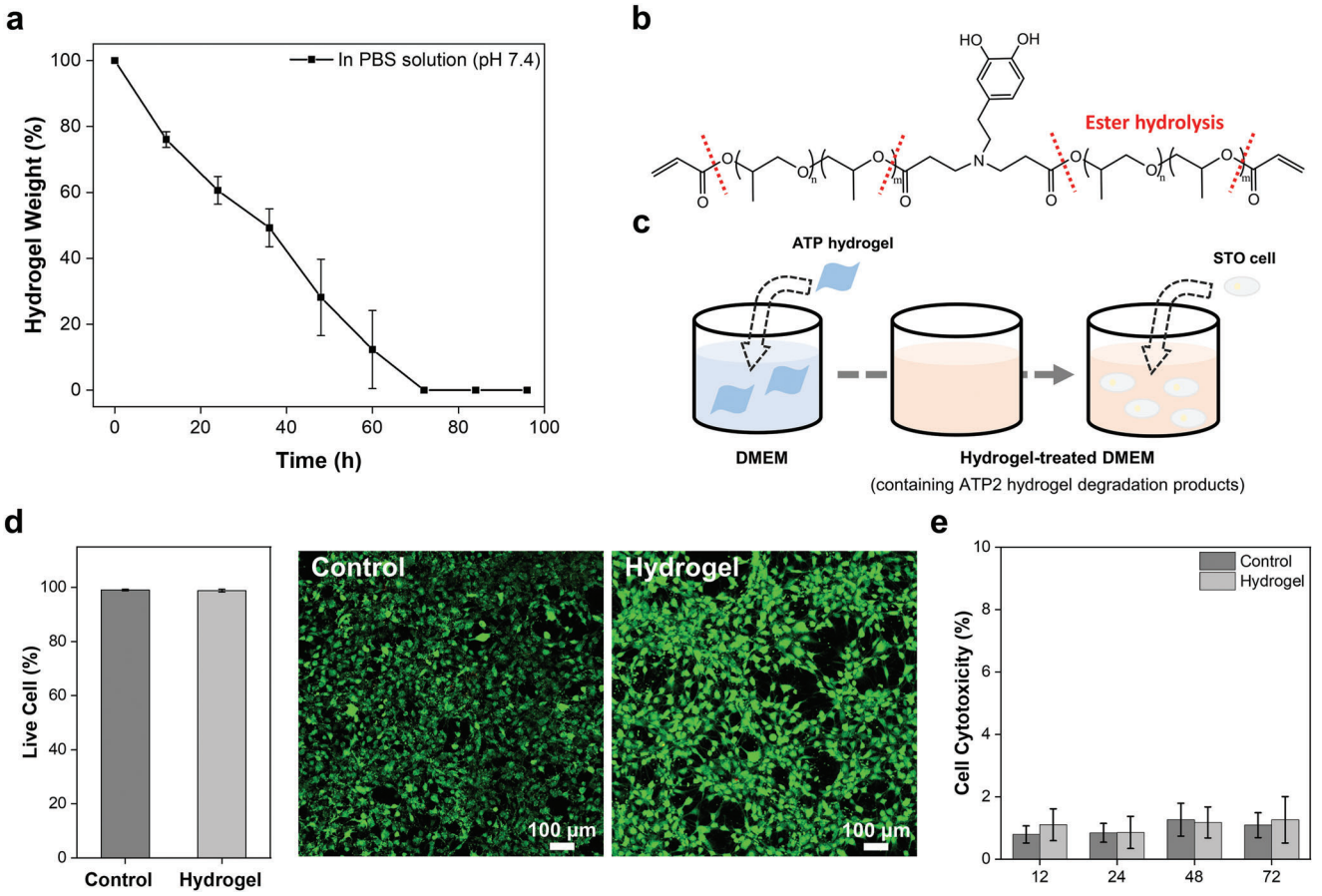

Figure 8. In vitro biocompatibility of ATP hydrogel. a) Biodegradation in PBS solution (pH 7.4) for 96 h. b) Schematic of the degradation mechanism of TPDC. c) Schematic of in vitro biocompatibility test process. d) Live/dead cell staining 72 h after incubation and e) potential toxicity over time.

were conducted 11 d post-implantation to evaluate tissue regeneration. In comparison to the control group, the hydrogel-treated group exhibited accelerated healing speed (**Figure 9a**) and a significantly higher level of the angiogenesis marker, vascular endothelial growth factor (VEGF) (Figure 9b). In H&E staining tests, the hydrogel-treated group demonstrated tissue (epidermis and dermis) thickness similar to that of the normal (non-wounded) group, while the control group exhibited significant tissue thickening (Figure 9c,d). Masson's staining analysis revealed a significantly higher collagen deposition in the hydrogel-treated group than in the control group (Figure 9e,f). Collectively, these results demonstrate that the ATP hydrogel promotes tissue regeneration at the wound site.[45] The pH-sensitive AA can absorb excess exudates produced by the wounds. Furthermore, due to its robust tissue adhesion, the ATP hydrogel can securely adhere to the wound and stabilize the wound site. This capability enables the ATP hydrogel to protect the wound site, maintaining a moist environment and thereby accelerating wound healing.[46]

3. Conclusions

This study reports the synthesis of highly resilient DN hydrogel adhesives utilizing an acrylate-terminated and dopamine-modified crosslinker, TPDC, and linear PVI. The first network was formed through covalent bonding between AA and TPDC, and the second network was generated through noncovalent intermolecular interactions (hydrogen bonds, hydrophobic associations, cation–π interactions, π–π interactions and chain entanglement) between poly(AA), TPDC, and PVI. These covalent and noncovalent intermolecular interactions led to associated network structures, resulting in the ATP hydrogel with remarkable toughness and mechanical resilience. The polar groups of dopamine and imidazole within the ATP hydrogel formed strong bonds with tissues, ensuring robust adhesion even in wet conditions. The DN hydrogel adhesives, prepared with AA, TPDC, and PVI exhibited exceptional tissue adhesion, toughness, and mechanical resilience performances that are typically negatively correlated. The ATP hydrogel effectively sealed damaged tissues owing to its well-balanced mechanical performance, while the pH-sensitive AA promoted wound healing by maintaining a moist environment. Overall, this study presents a straightforward method for fabricating highly resilient hydrogel adhesives with adjustable mechanical properties, making them promising materials for wound dressings. With further exploration, the application of these proposed hydrogel adhesives could be extended to include wearable electronic devices.

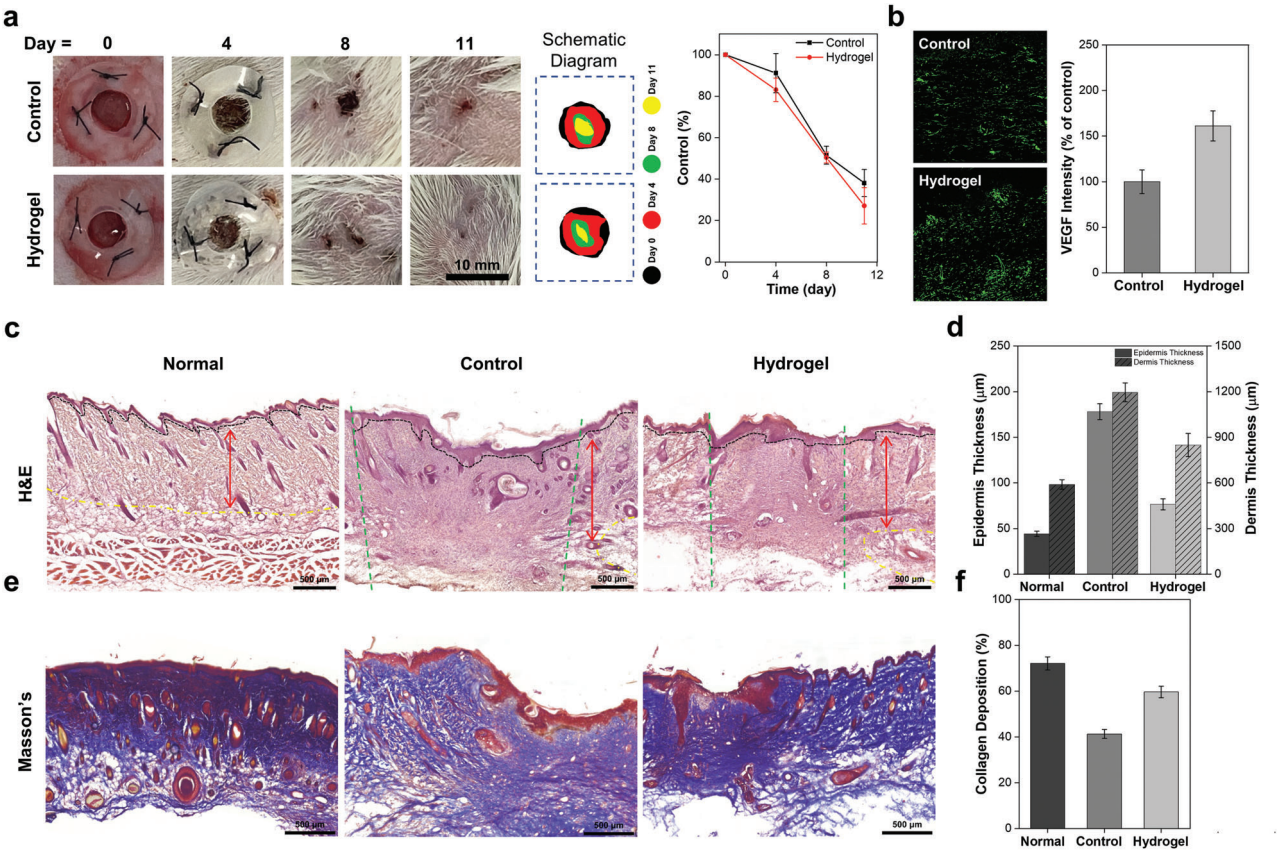

Figure 9. In vivo wound healing test. a) Effect of the ATP2 hydrogel on wound healing and remaining wound size over time. b) Immunohistochemistry staining images and VEGF antibody expression ratio. c) H&E staining images. Black and green dashed lines represent the boundary of the epidermis and wound site, respectively. Red arrows represent the dermis. Comparison of d) epidermis and dermis thickness values of non-wounded (normal) and wounded (control and hydrogel-treated) groups. e) Masson's trichrome staining images and comparison of f) collagen deposition in non-wounded (normal) and wounded (control and hydrogel-treated) groups.

4. Experimental Section

Materials: Tri (propylene glycol) diacrylate (TPGDA, average M_n 300) and tetraethyl thiuram disulfide (TETD, 97%) were purchased from Tokyo Chemical Industry Co., Ltd. 1-Vinyl imidazole (VI, 99%) and 2-hydroxy-4′-(2-hydroxyethoxy)−2-methylpropiophenone (Irgacure 2959, 98%) were purchased from Sigma-Aldrich. Dopamine hydrochloride (99%) was purchased from Alfa Aesar. Acrylic acid (AA, 99.5%), triethylamine (TEA, 99%), 2,2′-Azobisisobutyronitrile (AIBN, 98%), dimethyl sulfoxide (DMSO, 99.8%), N, N-dimethyl formamide (DMF, 99.5%), tert-butyl methyl ether (MTBE, 98.5%), and ether (99%) were purchased from Samchun Chemicals Co., Ltd. 10X Phosphate Buffered Saline (PBS) solution was purchased from Tech & Innovation. Dulbecco's modified Eagle medium (DMEM, #SH3243.01) was purchased from Hyclone Laboratories, Inc.

Preparation of Tri (propylene glycol) Diacrylate-Dopamine Crosslinker (TPDC): Dopamine hydrochloride (1.89 g, 10 mmol) and TPGDA (3.30 g, 11 mmol) were added to DMSO (12.12 g) under N_2 purging for 20 min at 25 °C. TEA (1.01 g, 10 mmol) was then added, and the mixture reacted at 80 °C for 12 h in dark conditions. After the reaction, TEA salt was removed through suction filtration. The solution was washed three times with MTBE, and the residual solvent was removed using a rotary evaporator at 60 °C for 6 h. A yellow-transparent liquid was obtained and stored at −20 °C.

Preparation of Poly(vinyl Imidazole) (PVI): PVI was prepared followed a previously reported method.[47] VI (2.35 g, 25 mmol), TETD (0.15 g, 0.5 mmol), and AIBN (0.16 g, 1 mmol) were added to DMF (10.0 g) under N_2 purging for 20 min. The solution reacted at 70 °C for 12 h. The resulting PVI was washed three times with ether, and the residual solvent was removed by vacuum evaporation at 25 °C.

Preparation of Acrylic acid-TPDC-PVI (ATP) Hydrogel: The pre-gel was synthesized in DMSO by free-radical photopolymerization. AA (1.0 g), TPDC (0.447 g, 0.7 mole% of AA), PVI (0.02 g, 2 wt.% of AA), and Irgacure 2959 (0.01 g, 1 wt.% of AA) were dissolved in DMSO (3.38 g). The mixture was poured into a Teflon mold sized 12 × 75 × 0.5 mm^3 (W × L × T) and subjected to UV irradiation (UV light-emitting diode lamp, intensity = 17 mW/cm^2) for 5 min. The resulting pre-gel was immersed in cold deionized water (DIW) for 12 h, with change to fresh DIW every 2 h. The DMSO extracted from the ATP pre-gel was measured by ^1H NMR, and its value was calculated using the ^1H NMR integral. (D_2O_n = 4.8 ppm peak integral at n h, $DMSO_n$ = 2.5 ppm peak integral at n h). To this end, ATP pre-gel (50 mg) was immersed in D_2O (1 mL) for 12 h, with the D_2O replaced every 2 h. Hydrogels with different PVI contents (0, 1, 3, and 4 wt.%) were prepared following the same procedure. The hydrogel with x wt.% of PVI was denoted as the ATPx hydrogel. Unless specified otherwise, the ATP2 hydrogel was used.

$$\text{Solvent extraction} = \frac{DMSO_n}{D_2O_n} \quad (1)$$

$$\text{Extraction ratio } (\%) = \frac{E_n}{\sum E_n} \times 100 \quad (2)$$

Characterization of TPDC, PVI, and ATP Hydrogel: IR spectra were recorded using an FT-IR spectrometer (Nicolet iS20, Thermo Fisher Scientific) to analyze the reaction ratio of TPDC. ^{1}H NMR spectra were recorded using a 400-MHz NMR spectrometer (JNM-ECX400, JEOL) to verify the molecular structures of TPDC and PVI. All ^{1}H NMR samples were measured at 25 °C in DMSO-D6 (using 0.03% tetramethylsilane ($\delta = 0$ ppm) as the reference). X-ray photoelectron spectra were recorded using an XPS spectrometer (K-Alpha, Thermo Scientific) to examine the surface chemical composition of the ATP hydrogel, and lyophilized ATP gel was used for XPS analysis. A monochromatic Al Kα X-ray ($h\nu = 1486.6$ eV) source was used, operating at 12 kV and 72 W. The neutral C1s peak was used as a reference (set at 284.6 eV).

Swelling Property: A 12 × 12 mm (W × L) pre-gel sample was immersed in DMSO and DIW at 25 °C. The swelling ratio was calculated based on the weight and volume change of the pre-gel. The weight and volume of the gel immersed in the solvent for n h were designated weight$_n$ and volume$_n$, respectively. The water content of the ATPx hydrogel was calculated by the mass loss after lyophilization.

$$\text{Swelling ratio } (\%) = \frac{\text{weight, volume}_n}{\text{weight, volume of pre} - \text{gel}} \times 100 \quad (3)$$

$$\text{Water content } (\%) = \frac{\text{weight of hydrogel} - \text{weight of lyophilized hydrogel}}{\text{weight of hydrogel}} \times 100 \quad (4)$$

Mechanical Property: Tensile and cyclic tensile tests were conducted using a Texture Analyzer (TA.XT plus, Stable Micro Systems) at 25 °C. The tensile tests were conducted at a rate of 100 mm/min. For the crack tip tensile tests, a knife was used to generate 1 mm crack tip in the center of the hydrogel. The cyclic tensile tests were conducted at a rate of 100 mm/min and repeated without rest. The strain rate in the cyclic tensile tests was set as 200%, 400%, 600%, and 700%. The residual strain and resilience values were calculated based on the initial loading-unloading curve.

$$\text{Resilience } (\%) = \frac{\int_{\text{unloading}} \sigma d\varepsilon}{\int_{\text{loading}} \sigma d\varepsilon} \times 100 \quad (5)$$

Adhesion Performance: Lap shear tests were conducted using a Texture Analyzer (TA.XT plus, Stable Micro Systems) at 25 °C and a rate of 50 mm/min. ATP hydrogel with 20 mm (L) and porcine skin with 25 × 50 mm^2 (W × L) were used. Before attaching the hydrogel, the substrate surface was thoroughly wetted with DIW. The ATP hydrogel was attached by applying a pressure of 1 kPa for 10 s. The sample was stored in a stainless tray with a cover at 25 °C with DIW sprayed to maintain a wet environment. Unless specified otherwise, the tests were conducted 3 h after adhesion.

Burst Pressure: A biopsy punch was used to introduce a 4 mm hole in the porcine skin. The skin was sprayed with DIW, and 1 × 1 mm^2 (W × L) ATP hydrogel was adhered to the hole. The porcine skin was then placed in a customized apparatus with an air flow of 50 cc/min. The pressure was measured using a manometer.

In Vitro Biodegradation: The lyophilized ATP hydrogel (30 mg) was immersed in 1 × PBS solution (5 mL, pH 7.4) at 36 °C for 4 d. After immersion for a 96 h, the ATP hydrogel was washed with DIW. The degradation rate of the ATP hydrogel was calculated considering the mass loss after lyophilization.

Cell Culture: To prepare hydrogel-treated media, the lyophilized ATP hydrogel (0.5 mg) was immersed in DMEM (1 mL) at 37° C for 4 d. STO cells were cultured in DMEM (10% FBS, 1% antibiotics) at 37 °C with 5% CO_2. Once the cells reached 80% confluence, the medium was replaced with hydrogel-conditioned DMEM and incubated. Pristine DMEM was used as the control. Details of the in vitro test methods can be found in Supporting Information.

In Vivo Wound Healing: All animal experiments were approved by the Institutional Animal Care and Use Committee of Seoul National University (SNU-230127-1). Six-week-old male Sprague Dawley rats were anesthetized with a mixture of Alfaxan (80 mg k^{-1}g) and xylazine HCl (10 mg k^{-1}g). Circular wounds with a diameter of 6 mm were created on the rats' backs using a biopsy punch, followed by suturing with a silicon wound splint. In the hydrogel-treated group, the ATP hydrogel was implanted and dressed in a Tegaderm film. In the control group, only the Tegaderm film was implanted. Tissue regeneration and vasculogenesis were monitored (0, 4, 8, and 11 d after implantation), and the wounded skin was harvested 11 d after implantation. Details regarding the staining test methods can be found in Supporting Information.

Supporting Information

Supporting Information is available from the Wiley Online Library or from the author.

Conflict of Interest

The authors declare no conflict of interest.

Data Availability Statement

The data that support the findings of this study are available from the corresponding author upon reasonable request.

Keywords

bioadhesive, crosslinking agent, dopamine, double-network, hydrogels

Received: October 2, 2023
Revised: January 13, 2024
Published online:

[1] H. Yuk, J. Wu, X. Zhao, *Nat. Rev. Mater.* **2022**, *7*, 935.
[2] G. Y. Han, S. K. Hwang, K. H. Cho, H. J. Kim, C. S. Cho, *Biomater. Res.* **2023**, *27*, 57.
[3] J. Deng, Y. Tang, Q. Zhang, C. Wang, M. Liao, P. Ji, J. Song, G. Luo, L. Chen, X. Ran, Z. Wei, L. Zheng, R. Dang, X. Liu, H. Zhang, Y. S. Zhang, X. Zhang, H. Tan, *Adv. Funct. Mater.* **2019**, *29*, 1809110.
[4] X. Chen, J. Zhang, G. Chen, Y. Xue, J. Zhang, X. Liang, I. M. Lei, J. Lin, B. B. Xu, J. Liu, *Adv. Funct. Mater.* **2022**, *32*, 2270168.
[5] X. Deng, B. Huang, Q. Wang, W. Wu, P. Coates, F. Sefat, C. Lu, W. Zhang, X. Zhang, *ACS Sustainable Chem. Eng.* **2021**, *9*, 3070.
[6] J. A. Cintron-Cruz, B. R. Freedman, M. Lee, C. Johnson, H. Ijaz, D. J. Mooney, *Adv. Mater.* **2022**, *34*, 2205567.
[7] J. Mo, Y. Dai, C. Zhang, Y. Zhou, W. Li, Y. Song, C. Wu, Z. Wang, *Mater. Horiz.* **2021**, *8*, 3409.
[8] Z. Yang, R. Huang, B. Zheng, W. Guo, C. Li, W. He, Y. Wei, Y. Du, H. Wang, D. Wu, H. Wang, *Adv. Sci.* **2021**, *8*, 2003627.
[9] T. Chen, Y. Chen, H. U. Rehman, Z. Chen, Z. Yang, M. Wang, H. Li, H. Liu, *ACS Appl. Mater. Interfaces* **2018**, *10*, 33523.
[10] Y. Hao, C. Yuan, J. Deng, W. Zheng, Y. Ji, Q. Zhou, *ACS Appl. Mater. Interfaces* **2022**, *14*, 16006.
[11] J. Yu, Y. Qin, Y. Yang, X. Zhao, Z. Zhang, Q. Zhang, Y. Su, Y. Zhang, Y. Cheng, *Bioact. Mater.* **2022**, *19*, 703.
[12] K. Zhao, B. Li, Y. Sun, B. Jia, J. Chen, W. Cheng, L. Zhao, J. Li, F. Wang, J. Su, J. Sun, B. Han, Y. Liu, H. Zhang, K. Liu, *Adv. Funct. Mater.* **2023**, *33*, 2301025.
[13] Y. Hong, F. Zhou, Y. Hua, X. Zhang, C. Ni, D. Pan, Y. Zhang, D. Jiang, L. Yang, Q. Lin, Y. Zou, D. Yu, D. E. Arnot, X. Zou, L. Zhu, S. Zhang, H. Ouyang, *Nat. Commun.* **2019**, *10*, 2060.

[14] M. Xu, Y. Miao, J. Yu, L. Zhang, *Adv. Mater. Interfaces* **2021**, *8*, 2101131.
[15] K. Chen, Z. Wu, Y. Liu, Y. Yuan, C. Liu, *Adv. Funct. Mater.* **2021**, *32*, 2109687.
[16] Y. Wang, D. Xiao, H. Yu, R. Ke, S. Shi, Y. Tang, Y. Zhong, L. Zhang, X. Sui, B. Wang, X. Feng, H. Xu, Z. Mao, *Compos. Pt. B-Eng.* **2022**, *235*, 109762.
[17] L. Han, K. Liu, M. Wang, K. Wang, L. Fang, H. Chen, J. Zhou, X. Lu, *Adv. Funct. Mater.* **2018**, *28*, 1704195.
[18] Q. Chen, H. Chen, L. Zhu, J. Zheng, *J. Mat. Chem. B* **2015**, *3*, 3654.
[19] T. L. Sun, T. Kurokawa, S. Kuroda, A. B. Ihsan, T. Akasaki, K. Sato, M. A. Haque, T. Nakajima, J. P. Gong, *Nat. Mater.* **2013**, *12*, 932.
[20] J. Slootman, C. J. Yeh, P. Millereau, J. Comtet, C. Creton, *Proc. Natl. Acad. Sci. U. S. A.* **2022**, *119*, e2116127119.
[21] J. P. Gong, *Soft Matter* **2010**, *6*, 2583.
[22] W. Dai, L. Zhang, Y. Yu, W. Yan, F. Zhao, Y. Fan, C. Cao, Q. Cai, X. Hu, Y. Ao, *Adv. Funct. Mater.* **2022**, *32*, 2200710.
[23] S. Li, G. Liu, H. Wen, G. Liu, H. Wang, M. Ye, Y. Yang, W. Guo, Y. Liu, *Adv. Funct. Mater.* **2022**, *32*, 2111747.
[24] L. Zhou, C. Dai, L. Fan, Y. Jiang, C. Liu, Z. Zhou, P. Guan, Y. Tian, J. Xing, X. Li, Y. Luo, P. Yu, C. Ning, G. Tan, *Adv. Funct. Mater.* **2021**, *31*, 2007457.
[25] G. Li, H. Zhang, D. Fortin, H. Xia, Y. Zhao, *Langmuir* **2015**, *31*, 11709.
[26] N. Varshney, A. K. Sahi, S. Poddar, N. K. Vishwakarma, G. Kavimandan, A. Prakash, S. K. Mahto, *ACS Appl. Mater. Interfaces* **2022**, *14*, 14033.
[27] L. Han, L. Yan, K. Wang, L. Fang, H. Zhang, Y. Tang, Y. Ding, L.-T. Weng, J. Xu, J. Weng, Y. Liu, F. Ren, X. Lu, *NPG Asia Mater.* **2017**, *9*, e372.
[28] X. Liu, J. Wu, K. Qiao, G. Liu, Z. Wang, T. Lu, Z. Suo, J. Hu, *Nat. Commun.* **2022**, *13*, 1622.
[29] S. D. Tobing, A. Klein, *J. Appl. Polym. Sci.* **2001**, *79*, 2230.
[30] G. Y. Han, J. Y. Park, T. H. Lee, M. B. Yi, H. J. Kim, *ACS Appl. Mater. Interfaces* **2022**, *14*, 36304.
[31] K. Noack, J. Kiefer, A. Leipertz, *ChemPhysChem* **2010**, *11*, 630.
[32] A. Eklund, H. Zhang, H. Zeng, A. Priimagi, O. Ikkala, *Adv. Funct. Mater.* **2020**, *30*, 2000754.
[33] Y. Zhou, M. Layani, S. Wang, P. Hu, Y. Ke, S. Magdassi, Y. Long, *Adv. Funct. Mater.* **2018**, *28*, 1705365.
[34] T. P. Sullivan, W. H. Eaglstein, S. C. Davis, P. Mertz, *Wound Repair Regen.* **2001**, *9*, 66.
[35] J. Saiz-Poseu, J. Mancebo-Aracil, F. Nador, F. Busque, D. Ruiz-Molina, *Angew. Chem., Int. Ed.* **2019**, *58*, 696.
[36] J. Zhang, Y. Wang, J. Zhang, I. M. Lei, G. Chen, Y. Xue, X. Liang, D. Wang, G. Wang, S. He, J. Liu, *Small* **2022**, *18*, 2201796.
[37] G.-Y. Han, H.-W. Kwack, Y.-H. Kim, Y. H. Je, H.-J. Kim, C.-S. Cho, *Carbohydr. Polym.* **2024**, *327*, 121634.
[38] H. Jeong, W. D. Wang, *Sens. Actuators, A* **2023**, *349*, 114083.
[39] Y. Mengüç, Y.-L. Park, H. Pei, D. Vogt, P. M. Aubin, E. Winchell, L. Fluke, L. Stirling, R. J. Wood, C. J. Walsh, *Int. J. Robot. Res.* **2014**, *33*, 1748.
[40] J. Kim, G. Zhang, M. Shi, Z. Suo, *Science* **2021**, *374*, 212.
[41] B. Ying, Q. Wu, J. Li, X. Liu, *Mater. Horiz.* **2020**, *7*, 477.
[42] H. Wang, X. Yi, T. Liu, J. Liu, Q. Wu, Y. Ding, Z. Liu, Q. Wang, *Adv. Mater.* **2023**, *35*, 2300394.
[43] H. Yuk, J. Wu, T. L. Sarrafian, X. Mao, C. E. Varela, E. T. Roche, L. G. Griffiths, C. S. Nabzdyk, X. Zhao, *Nat. Biomed. Eng.* **2021**, *5*, 1131.
[44] J. Qu, X. Zhao, Y. Liang, T. Zhang, P. X. Ma, B. Guo, *Biomaterials* **2018**, *183*, 185.
[45] E. Y. X. Loh, N. Mohamad, M. B. Fauzi, M. H. Ng, S. F. Ng, M. C. I. Mohd Amin, *Sci. Rep.* **2018**, *8*, 2875.
[46] H. C. Korting, C. Schollmann, R. J. White, *J. Eur. Acad. Dermatol. Venereol.* **2011**, *25*, 130.
[47] T. Xie, J. Ding, X. Han, H. Jia, Y. Yang, S. Liang, W. Wang, W. Liu, W. Wang, *Mater. Horiz.* **2020**, *7*, 605.